ACS APPLIED MATERIALS & INTERFACES

Research Article

www.acsami.org

# Impact of Aggregation on the Photochemistry of Fullerene Films: Correlating Stability to Triplet Exciton Kinetics

Emily M. Speller,[†] James D. McGettrick,[†] Beth Rice,[§] Andrew M. Telford,[§] Harrison K. H. Lee,[†] Ching-Hong Tan,[‡] Catherine S. De Castro,[†] Matthew L. Davies,[†] Trystan M. Watson,[†] Jenny Nelson,[§] James R. Durrant,[†,‡] Zhe Li,*[,†] and Wing C. Tsoi*[,†]

[†]SPECIFIC, College of Engineering, Swansea University, Bay Campus, Fabian Way, Swansea SA1 8EN, United Kingdom

[‡]Department of Chemistry and Centre for Plastic Electronics and [§]Department of Physics and Centre for Plastic Electronics, Imperial College London, London SW7 2AZ, United Kingdom

Supporting Information

**ABSTRACT:** The photochemistry and stability of fullerene films is found to be strongly dependent upon film nanomorphology. In particular, $PC_{61}BM$ blend films, dispersed with polystyrene, are found to be more susceptible to photobleaching in air than the more aggregated neat films. This enhanced photobleaching correlated with increased oxygen quenching of $PC_{61}BM$ triplet states and the appearance of a carbonyl FTIR absorption band indicative of fullerene oxidation, suggesting $PC_{61}BM$ photo-oxidation is primarily due to triplet-mediated singlet oxygen generation. $PC_{61}BM$ films were observed to undergo photo-oxidation in air for even modest (≤40 min) irradiation times, degrading electron mobility substantially, indicative of electron trap formation. This conclusion is supported by observation of red shifts in photo- and electro-luminescence with photo-oxidation, shown to be in agreement with time-dependent density functional theory calculations of defect generation. These results provide important implications on the environmental stability of $PC_{61}BM$-based films and devices.

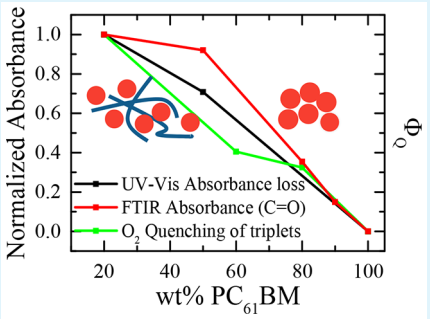


**KEYWORDS:** *triplet exciton kinetics, aggregation, fullerenes, photo-oxidation, stability, $PC_{61}BM$*

## INTRODUCTION

Fullerenes and their derivatives have become an important class of n-type semiconducting material since their discovery and large scale production. Their unique optical and electronic properties, including their desirable electron affinity and mobility, suitable energetic bandgap, ease of processing, and good compatibility with other semiconducting materials, have enabled them to be an attractive candidate for a broad range of applications,[1−7] in particular their almost ubiquitous use in solution processed organic photovoltaic cells (OPV).[8−10]

OPV is attracting great interest for low cost photovoltaic solar cells, with power conversion efficiencies now >11%, exceeding the threshold of commercial viability for some applications.[11−14] However, their relatively poor device lifetimes, particularly under typical operating conditions (light, heat, oxygen, and humidity), have limited their potential commercialization.[15−18] Recently, device degradation due to exposure to light and oxygen has become a widely recognized challenge within the community, as low cost, flexible OPV products typically employ plastic based encapsulation which offer only partial barriers to oxygen ingress. While significant research efforts have been dedicated to understanding and addressing the challenge of photochemical degradation of OPV, most of these research efforts have either been focused on donor polymers and/or device electrodes and interlayers.[19−27] On the other hand, the photochemical stability of fullerenes and their derivatives, such as phenyl-C61-butyric acid methyl ester ($PC_{61}BM$), one of the most commonly used electron accepting materials for OPV, has to date received considerably less investigation.

It has previously been shown that both C60 and $PC_{61}BM$ are susceptible to photodegradation upon extended light and oxygen exposure.[28−32] However, the mechanism of this degradation and its relevance to OPV device operating conditions have not been fully established. Most previous studies have used extreme light exposure or environmental conditions not relevant to device operation. Regarding the mechanism, it is not known whether the degradation is due to oxygen doping or a chemical oxidation.[18] It has also been demonstrated that a very low level of chemically induced oxidation to a customized fullerene derivative can significantly reduce the device efficiency of OPV[33] and that electron transfer from fullerene to oxygen, resulting in superoxide formation, can have a significant impact on the photochemical stability of donor polymers.[19] Moreover, as several air-stable polymers have been developed for OPV,[24,27] it is becoming even more important to study the photostability of fullerenes. These studies thus suggest that, as one of the most commonly used

Received: March 7, 2017
Accepted: June 12, 2017
Published: June 12, 2017





DOI: 10.1021/acsami.7b03298
ACS Appl. Mater. Interfaces XXXX, XXX, XXX−XXX

acceptor materials, elucidation of the photochemical stability of fullerenes and their derivatives is a key challenge for optimization of OPV stability.

For OPV, the fullerene is normally mixed with donor polymers to form an optimized blend morphology, typically on the nanoscale, further tunable by solution and film processing techniques such as thermal/vapor annealing and addition of solvent additives.[34−36] Furthermore, numerous studies have reported the strong links between the efficient operation of OPV and the presence of both intimately mixed polymer: fullerene domains and relatively pure, aggregated fullerene domains.[37−39] Several reports have also highlighted large differences between the photophysics of dispersed and aggregated (more crystalline) $PC_{61}BM$, with the latter exhibiting enhanced visible light absorption and the absence of long-lived triplet states. Most OPV employing $PC_{61}BM$ as an acceptor will include both molecularly dispersed and aggregated $PC_{61}BM$'s; however, to date there have been no studies addressing the impact of this aggregation upon its susceptibility to photodegradation.

Here we present a detailed study of the photodegradation, under light and oxygen exposure, of neat, aggregated films of $PC_{61}BM$ and films where $PC_{61}BM$ is dispersed in a polystyrene (PS) matrix. PS has previously been shown to be an effective matrix to disperse $PC_{61}BM$.[40−42] It has also been used as an additive to improve the performance of organic small molecule: fullerene OPV,[43] and blended with $PC_{61}BM$ to form the electron transport layer in "OPV type" perovskite solar cells with improved homogeneity and suppressed electron recombination.[44] Our results show that $PC_{61}BM$ can be easily photo-oxidized and that this photodegradation is increased when blended with PS, suggesting that less aggregated $PC_{61}BM$ is easier to photo-oxidize. Our results provide in-depth knowledge on this photodegradation which has important implications for the stability of fullerene based OPV, as well as perovskite solar cells employing $PC_{61}BM$ electron collection layers.

## METHODS

**Materials.** $PC_{61}BM$ was ordered from Solenne BV and used without further purification. The PS had a molecular weight of 210 kg/mol and polydispersity ∼2.0 and was ordered from Scientific Polymer Products, Inc.

**Film Preparation.** PS was dissolved in chlorobenzene (CB) at 8 mg/mL and mixed with the relevant amount of $PC_{61}BM$ powder to form the different wt % blend solutions (the concentration of the $PC_{61}BM$ in the solution was kept below 24 mg/mL). For neat films, the $PC_{61}BM$ powders were dissolved in chloroform (CF) at 24 mg/mL [and for attenuated total reflectance-Fourier transform infrared measurements (ATR-FTIR): it was 27 mg/mL] as the neat $PC_{61}BM$ solutions yielded better film homogeneity with CF rather than CB. The solutions were then spin-coated onto the substrates to form ∼100 nm thick films. Quartz (UV−vis absorbance), aluminum (ATR-FTIR), indium tin oxide (ITO; X-ray photoelectron spectroscopy (XPS)), and glass (photoluminescence (PL) and transient absorption spectroscopy (TAS)) substrates were used. All of the substrates were cleaned by sonicating in acetone and then isopropanol, followed by air plasma treatment.

**Devices Preparation.** Electron-only devices were fabricated with a structure of ITO/aluminum (Al)/$PC_{61}BM$/calcium (Ca)/Al. 50 nm Al was thermally evaporated onto cleaned ITO glass substrates at $2 \times 10^{-5}$ mbar. CB was first spin-coated on the ITO/Al substrates followed by the $PC_{61}BM$ solution, with concentration of 50 mg/mL in CB, forming a $PC_{61}BM$ layer with thickness ∼170 nm. The films were then photoaged. Finally, 30 nm Ca and 100 nm Al were sequentially thermally evaporated onto the $PC_{61}BM$ layers to complete the devices with an active area of 0.15 $cm^2$. All of the devices were encapsulated with glass slides and epoxy. Electroluminescence (EL) devices were fabricated by spin coating $PC_{61}BM$ solution (24 mg/mL in CF) onto PEDOT:PSS coated ITO substrates (thickness of $PC_{61}BM$ film ∼100 nm), followed by the same thermal evaporation of the top electrode and encapsulation, prior to measurement.

**Photoaging.** Photoaging of the films/devices was performed under ∼0.9−1 Sun AM1.5G in ambient conditions and temperature using a solar simulator, with no filters, for the aging time specified in the text.

**Characterization.** The UV−vis absorbance was calculated from the transmission and diffuse reflectance measurements performed on a UV-2600 Shimadzu UV−vis spectrophotometer with integrating sphere attachment.

ATR-FTIR spectra were acquired on a FTIR spectrometer (PerkinElmer Frontier) with a germanium ATR top plate with crystal diameter 1.3 mm. The spectra were processed from raw data that consisted of 4 scans and 1 $cm^{-1}$ resolution. The spectra were baseline corrected in the Spectrum 10 software. Three spectra were taken and averaged for each sample region. The FTIR absorbance of the C═O stretch of the side chain of $PC_{61}BM$ was used to normalize the data, as it is not that sensitive to the photoaging.

XPS spectra were obtained using a Kratos Axis Supra (Kratos Analytical, Manchester, U.K.) using a monochromated Al K$\alpha$ source. All spectra were recorded using a charge neutralizer to limit differential charging. As no adventitious carbon peak is present in the bulk, the main carbon peak is charge referenced to 284.5 eV.[45,46] Depth profiles were generated by rastering a 2.5 kV $Ar_{500}^+$ beam over a 2 × 2 mm area. The etching conditions were carefully tuned, so that the chemistry of the films was not significantly altered by the etching. During depth profiles, a 110 $\mu$m aperture was used to limit any influence of crater edges. Wide scans were recorded with a pass energy of 160 eV and dwell time of 198 ms and high resolution data at a pass energy of 40 eV. The data was fitted using CASA XPS with Shirley backgrounds. Film thicknesses, and hence etch rates, were confirmed after each etch by measurement with a Dektak 150 stylus profilometer.

For TAS measurements, the spectrum and decays of the photoinduced species of the films were measured using microsecond transient absorption spectroscopy. The films were selectively pumped using a Nd:Yag laser (Oppolette) at 355 nm, with an intensity of 7 $\mu J.cm^{-2}$ and a repetition rate of 20 Hz. The transient data were probed at 700 nm. The measurements were performed under both nitrogen ($N_2$) and oxygen ($O_2$) environments. For more details on the TAS setup, refer to ref 47.

Electron-only devices: Current−voltage characterizations were performed by a Keithley 2400 source meter. Electrons were injected from the Ca/Al electrodes.

PL and EL spectra were measured using a spectrograph (Andor Shamrock 303) combined with an InGaAs photodiode array (Andor iDUS 491) cooled to −90 °C, calibrated with a Bentham CL2 quartz halogen lamp with known emission spectrum. EL spectra were collected at an injection current density of 200 $mA/cm^2$. PL spectra were collected using a 473 nm continuous wave laser as the excitation source, with optical power density of 20−65 $mW/cm^2$. Data for both fresh and photoaged $PC_{61}BM$ devices were collected on three different pixels (or areas) on two separate devices.

**Modeling.** Electronic structure calculations of the epoxides of $PC_{61}BM$ were carried out using density functional theory. First, all possible single epoxides (one epoxide defect on one of the 6−6 carbon bonds of $PC_{61}BM$) were calculated and then a number of double epoxides, as well as the diols and carbonyl defects, which may be expected to develop from epoxide following the mechanism published by Xiao et al.[48] In each case, the total energy of the optimized defected structures was calculated to find the lowest energy structures. All calculations were done at the B3LYP level of theory using the 6-31g* basis set. For the optical spectra calculations, the lowest energy structures for each defect were chosen. Time-dependent density functional theory (TD-DFT) calculations were performed on the structures with Gaussian 09 in order to extract the oscillator strength and transition energy of the first 100 transitions. These were used to obtain an emission spectrum using


DOI: 10.1021/acsami.7b03298
ACS Appl. Mater. Interfaces XXXX, XXX, XXX−XXX

$$\varepsilon(E) = \frac{N}{\sigma}\sum_{i}^{N} f_i D(E, E_i) E_i^2 \exp\left(-\frac{E_i}{kT}\right) \quad (1)$$

where $N$ is the number of transitions, $\sigma$ is a width defined by the energy, and $f_i$ and $E_i$ are the oscillator strength and the energy of the $i$th excitation, respectively. $D$ is a line shape function defined by

$$D(E, E_i) = \exp\left[\left(\frac{E - E_i}{\sigma}\right)\right]^2 \quad (2)$$

## RESULTS AND DISCUSSION

**Spectroscopic Studies of Photo-oxidation.** First, UV−vis absorbance measurements were taken as photobleaching is routinely used to probe the degradation of conjugated polymers.[23,24] Figure 1a shows the normalized UV−vis

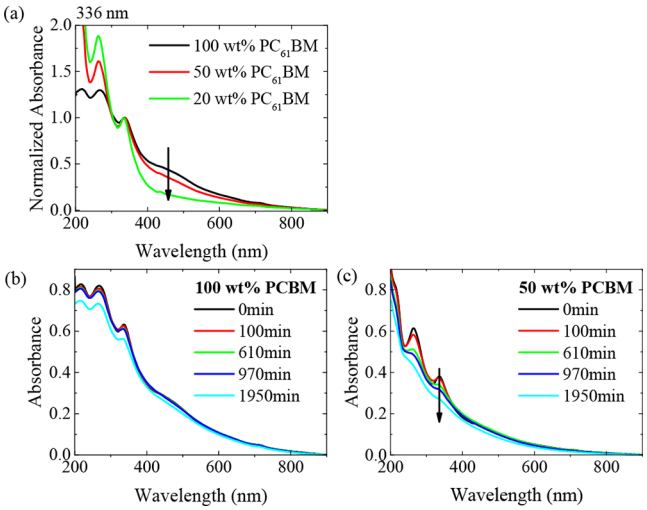


**Figure 1.** UV−vis absorption spectra of (a) neat $PC_{61}BM$ and $PC_{61}BM$:PS films, without any degradation (normalized at 336 nm), and of (b) 100 and (c) 50 wt % $PC_{61}BM$ films, as a function of photoaging time under AM1.5 irradiation and air exposure.

absorbance spectra of unaged neat $PC_{61}BM$ and $PC_{61}BM$:PS films. As the wt % $PC_{61}BM$ is reduced, the absorbance from 350−750 nm reduces relative to that of the 336 nm peak. As reported previously, this result is consistent with $PC_{61}BM$ molecules being less aggregated in the lower wt % blend films.[49,50] The PS film has a negligible absorbance over this spectral range. Panels b and c of Figure 1 compare the photobleaching of a neat $PC_{61}BM$ film and a 50 wt % $PC_{61}BM$ film as a function of photoaging time in ambient air under AM1.5 irradiation over 1950 min (32.5h). It can be clearly observed that, while there is only minimal photobleaching of the neat $PC_{61}BM$ film, the 50 wt % $PC_{61}BM$ film was significantly photobleached, indicating the less aggregated $PC_{61}BM$ film is more susceptible to photobleaching.

Next, the chemical nature of this photodegradation was investigated using ATR-FTIR spectroscopy. Panels a and b of Figure 2 compare the normalized ATR-FTIR absorbance spectra of a neat $PC_{61}BM$ film and 50 wt % $PC_{61}BM$ film, respectively, as a function of photoaging time, probing in the region of the prominent $PC_{61}BM$ 1737 $cm^{-1}$ absorption peak, assigned to the C═O stretch of the ester functional group of the $PC_{61}BM$ side chain.[29] We observed that the magnitude of a new peak at 1782 $cm^{-1}$ increases (relative to the 1737 $cm^{-1}$) with increased photoaging time (observable from ∼100 min)

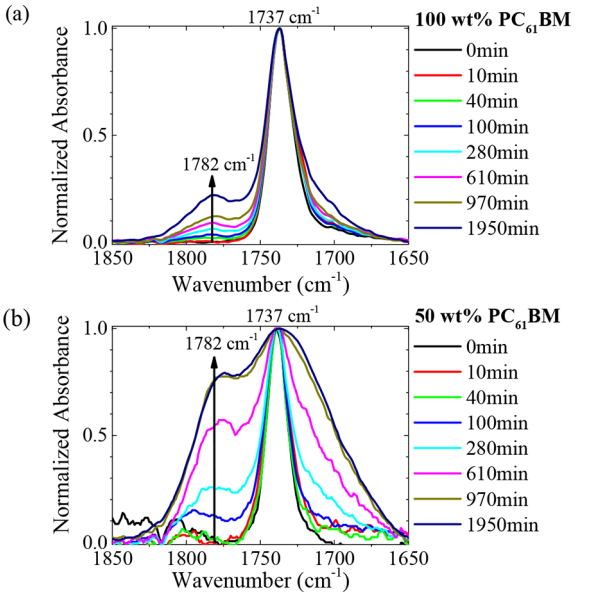


**Figure 2.** Normalized ATR-FTIR absorbance spectra of (a) neat $PC_{61}BM$ and (b) 50 wt % $PC_{61}BM$ films, respectively, as a function of photoaging time.

for the neat $PC_{61}BM$ film. The peak at 1782 $cm^{-1}$ has been assigned previously to the formation of carbonyls (the stretching mode of C═O)), likely associated with oxidation at the $PC_{61}BM$ cage.[28,51] Interestingly, the relative magnitude of this peak is significantly higher for the 50 wt % $PC_{61}BM$ film with the same photoaging time (0.80 vs 0.22 when they were photoaged for 1950 min). These results are consistent with the less aggregated $PC_{61}BM$ film being significantly easier to photo-oxidize, which matches with its higher tendency to photobleach. FTIR signals measured from neat and photoaged PS films were negligible (SI, Figure S1).

Further chemical analysis of this $PC_{61}BM$ photo-oxidation was undertaken using XPS, a surface sensitive technique. Figure 3a compares the XPS oxygen 1s envelope (O(1s)) of a neat $PC_{61}BM$ film and a 40 wt % $PC_{61}BM$ film, before and after 920 min of photoaging. It shows that the amount of measured oxygen increases after the photoaging, with significantly more oxygen observed for the photoaged 40 wt % $PC_{61}BM$ film than the neat film. (No O(1s) signal was observed from neat, fresh, or photoaged PS film.) Panels b and c of Figure 3 show the XPS spectra for the carbon 1s envelope (C(1s)) of neat $PC_{61}BM$ and 40 wt % $PC_{61}BM$ films, both photoaged for 920 min. The C(1s) envelope can be fitted with a number of peaks for different carbon environments (SI, Table S1). For the photoaged neat $PC_{61}BM$ film, there is a minor increase in the magnitude of the peaks at 286.1 and 288.3 eV; the increase in both peaks is much larger for the photoaged 40 wt % $PC_{61}BM$ film (the XPS spectrum for pristine films can be found in SI, Figure S2). The broadened peak at 286.1 eV is consistent with oxidized species such as C−O−C (epoxide), C−O−H, or C−O, while and the peak at 288.3 eV is consistent with carbonyls such as C═O or O−C═O (including an expected contribution from the $PC_{61}BM$ ester side chain).[52,53] It has been suggested that $PC_{61}BM$ can be photo-oxidized to form epoxides, then diols, and then carbonyls under sufficient photoaging (see SI, Figure S3).[48] These data support this mechanism, and it is therefore likely that in addition to the carbonyl defects visible in the FTIR spectra there is a


DOI: 10.1021/acsami.7b03298
ACS Appl. Mater. Interfaces XXXX, XXX, XXX−XXX

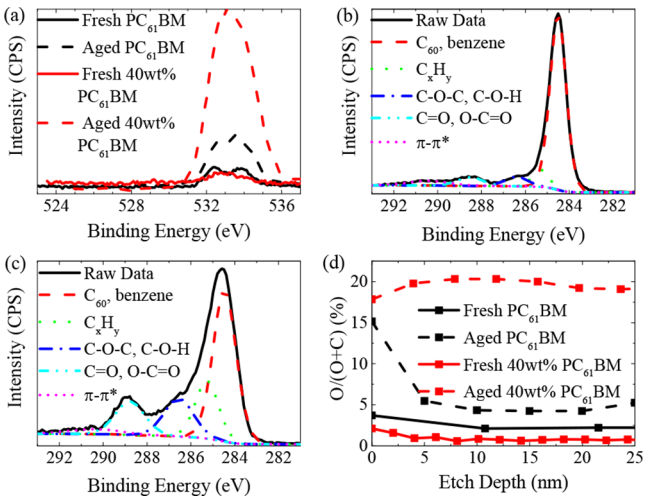


**Figure 3.** (a) XPS O(1s) spectrum of neat $PC_{61}BM$ and 40 wt % $PC_{61}BM$ films, before and after 920 min of photoaging, respectively; XPS C(1s) spectrum of (b) neat $PC_{61}BM$ and (c) 40 wt % $PC_{61}BM$ films, both after 920 min of photoaging; (d) atomic percentage of oxygen as a function of depth of $PC_{61}BM$ and 40 wt % $PC_{61}BM$ films, before and after 920 min of photoaging, respectively.

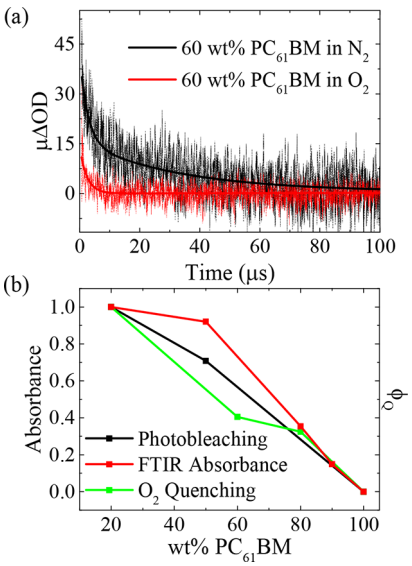


**Figure 4.** (a) Transient absorption decays of $PC_{61}BM$ triplet excitons pumped at 355 nm and probed at 700 nm of a 60 wt % $PC_{61}BM$ film in nitrogen and oxygen environments, respectively, (b) fractional loss of UV−vis absorbance, relative growth of C═O FTIR signal and relative fraction of excited states quenched by oxygen (calculated using eq 3), all normalized and as a function of wt % PC61BM, following photoaging of 1950 (UV−vis absorbance), 970 (FTIR), and 0 min (TAS).

substantial and probably larger population of epoxide defects. The C(1s) results show that the oxygens were chemically bound to the carbon atoms, and the level of photo-oxidation is much more significant for the less aggregated 40 wt % $PC_{61}BM$ film, consistent with the UV−vis and FTIR photoaging data (Figures 1 and 2, respectively).

XPS is capable of etching through films, with an argon gas cluster ion source gun, and quantifying the chemical composition with each etch, building up a depth profile. Figure 3d shows the atomic percentage of oxygen as a function of depth into the $PC_{61}BM$ and 40 wt % $PC_{61}BM$ films, before and after 920 min of photoaging, respectively. A 2.7% oxygen contribution would be expected from the ester group in neat $PC_{61}BM$ films. The lower oxygen percentage in the nonaged blend film is consistent with dilution of $PC_{61}BM$ by PS, which contains no oxygen. Interestingly, the photo-oxidation on the surface of the neat $PC_{61}BM$ film (oxygen atomic concentration ~15.2%) is much higher than in the bulk (~4.2%), while significant photo-oxidation occurs deep into the bulk for the 40 wt % $PC_{61}BM$ film (~17.9−20.3%).

**Investigation into the Photo-oxidation Mechanism.** In order to gain insight on the mechanism of the photo-oxidation, microsecond TAS measurements were performed on the $PC_{61}BM$ and PS:$PC_{61}BM$ films under nitrogen and oxygen. The films were selectively excited in the $PC_{61}BM$ absorption region (355 nm) and probed at its triplet $T_1-T_n$ absorption region (700 nm).[54] The decays were analyzed using a biexponential function and lifetimes calculated from the decay half-lives. On this time scale, singlet states have undergone intersystem crossing to triplet states as shown in the SI, Figure S4, and by Chow et al.[55] In addition, the decays measured under oxygen are quenched when compared to those under nitrogen (Figure 4a and Table 1), consistent with previous observations that triplet states are quenched by triplet ground state oxygen.[22] In a nitrogen atmosphere, the amplitude of photoinduced $PC_{61}BM$ $T_1-T_n$ absorption at ~0.6 $\mu$s (the instrument response time) was observed to increase with decreasing $PC_{61}BM$ content, with no signal apparent for the neat $PC_{61}BM$ film which was also unobservable by Chow et al.[55] (Figure S4) In all cases where $T_1-T_n$ absorption was observed, its decay kinetics were accelerated in the presence of oxygen.

Figure 4b and Table 1 show the relative fraction of excited states that were oxygen quenched ($\Phi_Q$) as a function of wt % $PC_{61}BM$ (assuming only triplet states are quenched). $\Phi_Q$ is calculated by

$$\Phi_Q = Y_{N_2}\Phi_{O_2} \quad (3)$$

where $Y_{N2}$ is the relative triplet yield in a nitrogen environment (determined from the $T_1-T_n$ absorption amplitude at 700 nm at ~0.6 s and corrected for the relative fraction of light absorbed by the individual films at the excitation wavelength) and $\Phi_{O2}$ is the efficiency of oxygen quenching given by

$$\Phi_{O_2} = \left(1 - \frac{\tau_{O_2}}{\tau_{N_2}}\right) \quad (4)$$

where $\tau_{O_2}$ and $\tau_{N_2}$ are the lifetimes of the triplets under nitrogen and oxygen environments, respectively. Lifetimes were calculated from the half-lives of fitted decays.

As the wt % $PC_{61}BM$ is reduced, the yield of triplets quenched by oxygen $\Phi_{O_2}$ increases. Since the triplet yield at low wt % $PC_{61}BM$ is significantly enhanced, while the $\Phi_{O_2}$ are comparable (see Table 1), the increase of relative fraction of excited states being oxygen quenched can be attributed primarily to the significantly enhanced triplet yield at low wt %. Besides, the triplet lifetimes remain comparable for all of the wt % (see Table 1), which further suggests that the relative fraction of excited states quenched by oxygen depends on the triplet yield. Note that the rate constant of oxygen quenching of the triplets ($k_{O_2}$) where


DOI: 10.1021/acsami.7b03298
ACS Appl. Mater. Interfaces XXXX, XXX, XXX−XXX

Table 1. Properties of the Triplet Kinetics in Blend $PC_{61}BM$ Films[a]

| wt % $PC_{61}BM$ | $\tau_{N2}$ ($\mu$s) | $\tau_{O2}$ ($\mu$s) | $Y_{N2}$ | $\Phi_{O2}$ | $k_{O2}$ ($\times 10^6$ $s^{-1}$) | $\Phi_Q$ |
|---|---|---|---|---|---|---|
| 80 | 9.1 ± 0.1 | 2.2 ± 0.2 | 34.0 | 0.76 ± 0.07 | 0.35 ± 0.04 | 26.0 ± 3.0 |
| 60 | 6.2 ± 0.1 | 2.4 ± 0.2 | 53.0 | 0.61 ± 0.04 | 0.25 ± 0.03 | 32.0 ± 4.0 |
| 20 | 6.8 ± 0.1 | 1.7 ± 0.1 | 107.0 | 0.74 ± 0.03 | 0.43 ± 0.02 | 80. ± 4.0 |

[a] $\tau_{N2}$ and $\tau_{O2}$ are the triplet lifetimes under nitrogen and oxygen respectively, $Y_{N2}$ is the relative triplet yield in a nitrogen environment, $\Phi_{O2}$ is the efficiency of oxygen quenching, $k_{O2}$ is the rate constant of oxygen quenching, and $\Phi_Q$ is the relative fraction of excited states oxygen quenched.

$$k_{O_2} = \frac{1}{\tau_{O_2}} - \frac{1}{\tau_{N_2}} \quad (5)$$

remains comparable for all of the wt % (see Table 1), implying the oxygen diffusion rates are similar for the different compositions.

Figure 4b shows a clear correlation between the relative fraction of excited states being oxygen quenched and the level of photo-oxidation of the $PC_{61}BM$ films as a function of $PC_{61}BM$ aggregation. It can be seen that our assays of C═O formation (on the $PC_{61}BM$ cage, 970 min) and loss of UV−vis absorbance (1950 min) both correlate with our TAS assay of the relative fraction of oxygen quenched excited states. The lower wt % $PC_{61}BM$ (less aggregated) exhibits a higher fraction of excited states that were oxygen quenched, more C═O formation, and a larger UV−vis absorbance loss.

**Impact of Photo-oxidation on Electrical and Optical Properties of Films.** The consequences of the $PC_{61}BM$ photo-oxidation on optoelectronic film properties were investigated in order to explore the relevance of $PC_{61}BM$ photo-oxidation to device function. To study the effect of the photo-oxidation on charge transport, the current density versus electric field of electron-only devices using $PC_{61}BM$ as the active layer were measured with different photoaging times (see Figure 5a). Interestingly, even with <40 min photoaging, the current density dropped by 4−5 times. It is reasonable that a small amount of photo-oxidation (undetectable by the optical techniques) is sufficient to cause a significant effect on the electron transport, since it is well-known that a small density of charge traps can cause a significant drop in charge carrier mobility.[56] While the nature of the defects responsible for electron mobility loss cannot be determined exactly from these data, calculations of defect energies and the impact of defects of different depth on mobility (SI, Table S2 and Figure S6) strongly suggest that relatively shallow defects, such as epoxides, are more likely to be responsible for the mobility loss than deep carbonyl defects. The loss in mobility is consistent with the XPS data of the $PC_{61}BM$ film with 1 h photoaging which also showed significant photo-oxidation on the surface layer (oxygen concentration ~9.6%; also see SI, Figure S5).

The impact of photodegradation on the optical and electronic properties of $PC_{61}BM$ was then further probed by photo- and electro-luminescence measurements and correlated with TD-DFT calculations. Figure 5b shows PL and EL spectra of $PC_{61}BM$ films and devices before and after the photoaging. Both the PL and EL shift to lower energies after photoaging, indicating the generation of intraband defect states that are radiatively coupled to ground. Interestingly, after 1 h of photoaging, the neat $PC_{61}BM$ film does not show a measurable red-shift in the PL but does have a significant red-shift in the EL spectrum (from 1.64 to 1.48 eV). It is likely that for the EL, the electrons are transported to the lowest lying defect states where the emission occurs. Therefore, the EL is dominated by the

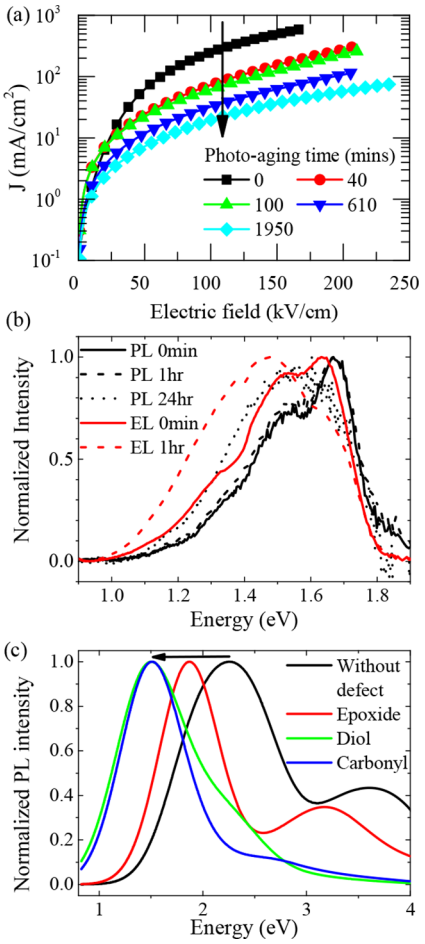


Figure 5. (a) Current density versus electric field of electron-only devices using $PC_{61}BM$ as the active layer with different photoaging times, (b) normalized PL and EL spectra of $PC_{61}BM$ films and devices, respectively, before and after the photoaging, and (c) calculated PL spectra (normalized) of $PC_{61}BM$ molecule with and without the oxidative defects.

emission of the oxidative defects; hence, it has a more pronounced red-shift. On the other hand, the PL signal is from all emissive species probed, where mainly the top surface of the degraded $PC_{61}BM$ film was photo-oxidized (see XPS section). For the $PC_{61}BM$ film photoaged for 24 h, the PL does red-shift (from 1.66 to 1.55 eV) which is consistent with more photo-oxidized defects/traps being formed (see FTIR section).

TD-DFT calculations were performed to model the effect of the photo-oxidation on the optical properties of $PC_{61}BM$. There was an observed red shift in the $PC_{61}BM$ PL spectra, modeled from a calculated deepening of the lowest unoccupied molecular orbital (LUMO) level, when epoxide, diol, or carbonyl defects were added (Figure 5c). The red shifts observed in the modeled PL spectra of $PC_{61}BM$ upon addition of oxygen to form defects are consistent with formation of the


DOI: 10.1021/acsami.7b03298
ACS Appl. Mater. Interfaces XXXX, XXX, XXX−XXX

electron traps. While the shape and the position of the calculated photo-oxidized peaks differ from experimentally obtained spectra due to a number of assumptions, such as neglect of the vibronic structure, the magnitude of the shift in luminescence peaks in calculated and experimental spectra can be compared. The experimental redshift of approximately 0.2 eV in the luminescence peak compares well with the shift expected due to the presence of epoxide defects and further supports the argument that these defects are likely to dominate the optoelectronic properties. The clear observation of PL and EL from defect states indicate that radiative recombination via trap states is not forbidden in the degraded $PC_{61}BM$ films or devices.

## DISCUSSION

Herein, we have shown that $PC_{61}BM$ is significantly easier to photobleach, the more it is dispersed in polystyrene, consistent with the formation of photo-oxidized species (e.g., carbonyl species). This enhanced photo-oxidation in more dispersed $PC_{61}BM$ films correlates with a higher yield of triplet states being formed. We also show that even neat $PC_{61}BM$ films can be photo-oxidized under 1 sun, with the current density in electron-only devices dropping by ∼5 times after only 40 min photoaging. The PL (and EL) spectra of the photoaged neat $PC_{61}BM$ films (and devices) are both significantly red-shifted, consistent with defect/trap emission. Using epoxides, diols, or carbonyls as the photo-oxidative defects for modeling, we found that all of the defects cause a red-shift in the PL spectra, due to a lower LUMO energy, in agreement with the experimental data. The shift is least pronounced in the case of epoxide defects, and the relatively mild effect of oxidation on electron mobility suggests that these shallower trap states may be the most active.

Although UV−vis absorbance is routinely used to probe degradation of conjugated polymers through photobleaching,[16−18] it is apparent from the electron transport data shown above that the functional electronic degradation of $PC_{61}BM$ films occurs even without observable change in absorbance. It is likely that epoxide/diol defects were formed prior to the formation of carbonyls;[57] therefore, the $PC_{61}BM$ and blend films may have already photo-oxidized before carbonyl formation was observed at ∼100 min by FTIR. This is supported by the significant drop in electron transport of the $PC_{61}BM$ electron-only devices, even after 40 min photoaging, and the significant surface oxidation observed via increased signal at the higher binding energies in the XPS C(1s) envelopes of neat $PC_{61}BM$ films after 1 h photoaging. (SI, Figure S5) Alternatively, it could also be possible that carbonyl defects were formed <100 min but the FTIR measurements were not sensitive enough to detect these. It should be noted that even the 90 wt % $PC_{61}BM$ film shows considerably more photo-oxidation than that of the 100 wt % $PC_{61}BM$ film (see Figure 4b), implying that the addition of a small wt % of PS can have a considerable effect on the photo-oxidation of $PC_{61}BM$ films. The drop in electron transport after 40 min shows that a small amount of electron traps can cause a significant drop in electrical transport, and importantly, for the first time, we show that neat $PC_{61}BM$ films can be degraded very easily under 1 sun conditions, unlike previous studies which use harsh conditions that may not be directly relevant to the illumination conditions for solar cells.[28−30]

TAS has been applied to study the photo-oxidation of conjugated polymers, and it has been suggested that photo-oxidation of some donor polymers is triplet-mediated,[23] with polymer triplet lifetimes increasing with lower polymer crystallinity.[24] Here, a strong correlation was found between the yield of triplets being oxygen quenched and the level of photo-oxidation of the $PC_{61}BM$ films as a function of $PC_{61}BM$ aggregation. This is consistent with triplet-mediated photo-oxidation, similar to that suggested as the cause of photo-degradation in some donor polymers.[23] This suggests that the degradation mechanism at play is singlet oxygen generation via the triplet excitons (Figure 6), whereby $PC_{61}BM$ triplets are

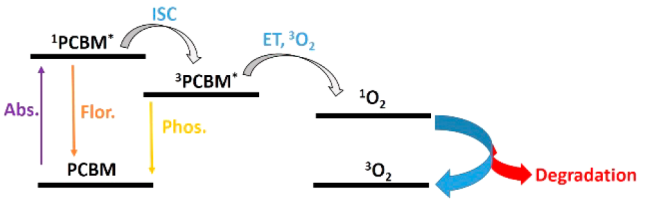


**Figure 6.** Model used to describe the possible degradation mechanism of $PC_{61}BM$ via triplet-mediated singlet oxygen generation.

formed via intersystem crossing (ISC) from the $PC_{61}BM$ singlet state after the absorption of photons. These triplet states can be quenched by molecular oxygen, via energy transfer, to generate highly reactive singlet oxygen, which causes the photo-oxidation of the $PC_{61}BM$. The top surface of the neat $PC_{61}BM$ film could be less aggregated than the bulk as it is exposed to air on one side and so has fewer neighboring molecules for aggregation. Therefore, it is easier to form triplets which lead to the photo-oxidation, which could explain the photo-oxidation observed on the surface of the neat $PC_{61}BM$ film (Figure 3d). TAS may not be sensitive enough to probe this small amount of triplets at the surface, consistent with negligible triplet absorption of the neat $PC_{61}BM$ film.

We also calculate the C−O:C═O ratio as estimated from the C(1s) envelope and total measured oxygen as a function of etch depth for the degraded blend film (see the SI, Figure.S7). The C−O:C═O ratio is quite constant up to 60 nm below the surface. At a depth of >60 nm, the C−O:C═O increases slightly together with less oxidation, which is consistent with epoxide formation first. It is reasonable to have less photo-oxidation at the deeper part of the film, as oxygen will be relatively more difficult to get to the regions. As the difference in the C−O:C═O is small, the photo-oxidation should not be dominated by the penetration of oxygen. This result also implies that the significant difference in photo-oxidation between the films should also not be related to the penetration of oxygen (consistent with their similar rate constants of oxygen quenching) but on the difference in the yield of triplets being oxygen quenched.

In donor/acceptor blends, the oxygen quenching of polymer triplets generated by the nongeminate recombination of dissociated polarons was shown to be the dominant pathway to photo-oxidation, but there is also an additional contribution from those triplets directly generated from singlet excitons by intersystem crossing.[23] However, the $PC_{61}BM$ triplet states were not taken into consideration for these systems. Research efforts to increase polymer stability have been making progress; thieno[3,2-*b*]thiophene−diketopyrrolopyrrole (DPP-TT-T) for example was shown to be very stable under white LED light irradiation (∼80 mW $cm^{-2}$) under a pure oxygen environment for over 250 h.[24] As polymer stability increases, the


DOI: 10.1021/acsami.7b03298
ACS Appl. Mater. Interfaces XXXX, XXX, XXX−XXX

contribution from these $PC_{61}BM$ triplets could well play a bigger role in singlet oxygen generation, and hence photo-oxidation.

In OPV devices, it has been reported that the active layer is composed of a finely intermixed polymer/fullerene phase where the fullerene is dispersed as well as relatively pure aggregated $PC_{61}BM$ domains.[38] The yield of $PC_{61}BM$ triplet states is likely to show a complex dependence on this nanomorphology, as well as on blend energetics. It is for example uncertain whether charge recombination in blends can yield $PC_{61}BM$ triplets in addition to polymer triplets.[23,58] The triplet energies of polymers and fullerenes are typically 0.9−1.2 and ∼1.5 eV, respectively;[55] therefore, energetically polymer triplets are more favorable to form. However, fullerene triplets have been observed in the blend with photoactive polymers.[59,60] It should also be noted that the permeability to molecular oxygen of the polystyrene matrix used in our samples is likely to differ from that of typical conjugated polymers. This may affect the rate of degradation in donor:$PC_{61}BM$ blends relative to our model system. Nevertheless, our observations herein are that (a) $PC_{61}BM$ triplet formation can lead to the generation of oxidizing species in the presence of oxygen (most likely singlet oxygen) and (b) $PC_{61}BM$ is susceptible to photo-oxidation by these oxidizing oxygen species which have important implications concerning the challenge of developing OPV devices with improved environmental stability.

## CONCLUSIONS

These studies give an in-depth understanding of the photo-oxidation of $PC_{61}BM$. As fullerene and fullerene:polymer films are commonly used for a broad range of optoelectronic devices (e.g., solar cells), our findings provide important insight into fullerene-based optoelectronics, highlighting that the photo-degradation of fullerene can be crucial to their stability.

## ASSOCIATED CONTENT

### Supporting Information

The Supporting Information is available free of charge on the ACS Publications website at DOI: 10.1021/acsami.7b03298.

ATR-FTIR spectra for PS neat film fresh and after photoaging, table with the XPS peak assignments, XPS spectra of fresh $PC_{61}BM$ and 40 wt % $PC_{61}BM$ films, possible photo-oxidation mechanism of the $PC_{61}BM$ film, transient absorption spectra of $PC_{61}BM$:PS films, XPS spectrum of $PC_{61}BM$ film after 1 h photoaging, calculated effect of different defect types on the LUMO energy of oxidized $PC_{61}BM$, simulated mobility in $PC_{61}M$ doped with different volume fraction of oxidized defects, and C−O:C═O ratio as estimated from the C(1s) envelope and total measured oxygen as a function of etch depth for degraded blend film. (PDF)

## AUTHOR INFORMATION


### Corresponding Authors

*E-mail: Z.Li@Swansea.ac.uk.

*E-mail: W.C.Tsoi@Swansea.ac.uk.

### ORCID

James R. Durrant: 0000-0001-8353-7345

Wing C. Tsoi: 0000-0003-3836-5139


### Notes

The authors declare no competing financial interest.

## ACKNOWLEDGMENTS

The authors would like to acknowledge the funding from the Sêr Cymru Programme: National Research Network in Advanced Engineering Materials (grant number NRN093), Welsh Assembly Government funded Sêr Cymru Solar Project, the J.R.D. funding from the EU Cheetah project, and EPSRC grants EP/M025020/1 (Supergen Solar Challenge) and EP/K030671/1. We also acknowledge Mr. LiFu Zhang for his assistance as a placement student. A.M.T. thanks the Imperial College Junior Research Fellowship scheme for funding. E.M.S. would also like to thank the Materials and Manufacturing Academy (M2A) for kindly providing publication costs.

## REFERENCES


(1) Chen, C.-C.; Dou, L.; Zhu, R.; Chung, C.-H.; Song, T.-B.; Zheng, Y. B.; Hawks, S.; Li, G.; Weiss, P. S.; Yang, Y. Visibly Transparent Polymer Solar Cells Produced by Solution Processing. *ACS Nano* **2012**, *6*, 7185−7190.

(2) Li, S.; Xue, D.; Xu, W.; Feng, Y.; Wang, J.; Zhang, G.; Meng, X.; Wang, C.; Song, Y.; Shu, C. Improving the Photo Current of the [60]PCBM/P3HT Photodetector Device by Using Wavelength-Matched Photonic Crystals. *J. Mater. Chem. C* **2014**, *2*, 1500.

(3) Ma, Z.; Zhao, J.; Wang, X.; Yu, J. Effect of Bulk and Planar Heterojunctions Based Charge Generation Layers on the Performance of Tandem Organic Light-Emitting Diodes. *Org. Electron.* **2016**, *30*, 136−142.

(4) Itoh, E.; Kanamori, A. Fabrication of Organic FETs Based on Printing Techniques and the Improvement of FET Properties by the Insertion of Solution-Processable Buffer Layers. *Jpn. J. Appl. Phys.* **2016**, *55*, 04EL06.

(5) Rambabu, G.; Nagaraju, N.; Bhat, S. D. Functionalized Fullerene Embedded in Nafion Matrix: A Modified Composite Membrane Electrolyte for Direct Methanol Fuel Cells. *Chem. Eng. J.* **2016**, *306*, 43−52.

(6) Prasad, B. B.; Kumar, A.; Singh, R. Molecularly Imprinted Polymer-Based Electrochemical Sensor Using Functionalized Fullerene as a Nanomediator for Ultratrace Analysis of Primaquine. *Carbon* **2016**, *109*, 196−207.

(7) Kulkarni, C. V.; Moinuddin, Z.; Agarwal, Y. Effect of Fullerene on the Dispersibility of Nanostructured Lipid Particles and Encapsulation in Sterically Stabilized Emulsions. *J. Colloid Interface Sci.* **2016**, *480*, 69−75.

(8) Khalil, A.; Ahmed, Z.; Touati, F.; Masmoudi, M. Review on Organic Solar Cells*2016 13th International Multi-Conference on Systems. Signals & Devices (SSD); IEEE* **2016**, 342−353.

(9) Lu, L.; Zheng, T.; Wu, Q.; Schneider, A. M.; Zhao, D.; Yu, L. Recent Advances in Bulk Heterojunction Polymer Solar Cells. *Chem. Rev.* **2015**, *115*, 12666−12731.

(10) Dou, L.; You, J.; Hong, Z.; Xu, Z.; Li, G.; Street, R. a.; Yang, Y. 25th Anniversary Article: A Decade of Organic/polymeric Photovoltaic Research. *Adv. Mater.* **2013**, *25*, 6642−6671.

(11) Laboratory, N. R. E. efficiency_chart.jpg (4190 × 2456) http://www.nrel.gov/ncpv/images/efficiency_chart.jpg (accessed Jan 6, 2017).

(12) Heliatek. Heliafilm technical data http://www.heliatek.com/en/heliafilm/technical-data (accessed Jan 6, 2017).

(13) Zhao, J.; Li, Y.; Yang, G.; Jiang, K.; Lin, H.; Ade, H.; Ma, W.; Yan, H. Efficient Organic Solar Cells Processed from Hydrocarbon Solvents. *Nat. Energy* **2016**, *1*, 15027.

(14) Liu, Y.; Zhao, J.; Li, Z.; Mu, C.; Ma, W.; Hu, H.; Jiang, K.; Lin, H.; Ade, H.; Yan, H. Aggregation and Morphology Control Enables Multiple Cases of High-Efficiency Polymer Solar Cells. *Nat. Commun.* **2014**, *5*, 5293.

(15) Mateker, W. R.; McGehee, M. D. Progress in Understanding Degradation Mechanisms and Improving Stability in Organic Photovoltaics. *Adv. Mater.* **2017**, *29*, 1603940.




DOI: 10.1021/acsami.7b03298
*ACS Appl. Mater. Interfaces* XXXX, XXX, XXX−XXX

(16) Jørgensen, M.; Norrman, K.; Krebs, F. C. Stability/degradation of Polymer Solar Cells. *Sol. Energy Mater. Sol. Cells* **2008**, *92*, 686−714.
(17) Jørgensen, M.; Norrman, K.; Gevorgyan, S. A.; Tromholt, T.; Andreasen, B.; Krebs, F. C. Stability of Polymer Solar Cells. *Adv. Mater.* **2012**, *24*, 580−612.
(18) Grossiord, N.; Kroon, J. M.; Andriessen, R.; Blom, P. W. M. Degradation Mechanisms in Organic Photovoltaic Devices. *Org. Electron.* **2012**, *13*, 432−456.
(19) Hoke, E. T.; Sachs-Quintana, I. T.; Lloyd, M. T.; Kauvar, I.; Mateker, W. R.; Nardes, A. M.; Peters, C. H.; Kopidakis, N.; McGehee, M. D. The Role of Electron Affinity in Determining Whether Fullerenes Catalyze or Inhibit Photooxidation of Polymers for Solar Cells. *Adv. Energy Mater.* **2012**, *2*, 1351−1357.
(20) Jørgensen, M.; Norrman, K.; Gevorgyan, S. A.; Tromholt, T.; Andreasen, B.; Krebs, F. C. Stability of Polymer Solar Cells. *Adv. Mater.* **2012**, *24*, 580−612.
(21) Manceau, M.; Bundgaard, E.; Carlé, J. E.; Hagemann, O.; Helgesen, M.; Søndergaard, R.; Jørgensen, M.; Krebs, F. C. Photochemical Stability of π-Conjugated Polymers for Polymer Solar Cells: A Rule of Thumb. *J. Mater. Chem.* **2011**, *21*, 4132.
(22) Distler, A.; Kutka, P.; Sauermann, T.; Egelhaaf, H.-J.; Guldi, D. M.; Di Nuzzo, D.; Meskers, S. C. J.; Janssen, R. A. J. Effect of PCBM on the Photodegradation Kinetics of Polymers for Organic Photovoltaics. *Chem. Mater.* **2012**, *24*, 4397−4405.
(23) Soon, Y. W.; Cho, H.; Low, J.; Bronstein, H.; McCulloch, I.; Durrant, J. R. Correlating Triplet Yield, Singlet Oxygen Generation and Photochemical Stability in Polymer/fullerene Blend Films. *Chem. Commun.* **2013**, *49*, 1291−1293.
(24) Soon, Y. W.; Shoaee, S.; Ashraf, R. S.; Bronstein, H.; Schroeder, B. C.; Zhang, W.; Fei, Z.; Heeney, M.; McCulloch, I.; Durrant, J. R. Material Crystallinity as a Determinant of Triplet Dynamics and Oxygen Quenching in Donor Polymers for Organic Photovoltaic Devices. *Adv. Funct. Mater.* **2014**, *24*, 1474−1482.
(25) Gevorgyan, S. A.; Medford, A. J.; Bundgaard, E.; Sapkota, S. B.; Schleiermacher, H.-F.; Zimmermann, B.; Würfel, U.; Chafiq, A.; Lira-Cantu, M.; Swonke, T.; Wagner, M.; Brabec, C. J.; Haillant, O.; Voroshazi, E.; Aernouts, T.; Steim, R.; Hauch, J. A.; Elschner, A.; Pannone, M.; Xiao, M.; Langzettel, A.; Laird, D.; Lloyd, M. T.; Rath, T.; Maier, E.; Trimmel, G.; Hermenau, M.; Menke, T.; Leo, K.; Rösch, R.; Seeland, M.; Hoppe, H.; Nagle, T. J.; Burke, K. B.; Fell, C. J.; Vak, D.; Singh, T. B.; Watkins, S. E.; Galagan, Y.; Manor, A.; Katz, E. A.; Kim, T.; Kim, K.; Sommeling, P. M.; Verhees, W. J. H.; Veenstra, S. C.; Riede, M.; Greyson Christoforo, M.; Currier, T.; Shrotriya, V.; Schwartz, G. An Inter-Laboratory Stability Study of Roll-to-Roll Coated Flexible Polymer Solar Modules. *Sol. Energy Mater. Sol. Cells* **2011**, *95*, 1398−1416.
(26) Peters, C. H.; Sachs-Quintana, I. T.; Kastrop, J. P.; Beaupré, S.; Leclerc, M.; McGehee, M. D. High Efficiency Polymer Solar Cells with Long Operating Lifetimes. *Adv. Energy Mater.* **2011**, *1*, 491−494.
(27) Adams, J.; Spyropoulos, G. D.; Salvador, M.; Li, N.; Strohm, S.; Lucera, L.; Langner, S.; Machui, F.; Zhang, H.; Ameri, T.; Voigt, M. M.; Krebs, F. C.; Brabec, C. J. Air-Processed Organic Tandem Solar Cells on Glass: Toward Competitive Operating Lifetimes. *Energy Environ. Sci.* **2015**, *8*, 169−176.
(28) Neugebauer, H.; Brabec, C.; Hummelen, J. C.; Sariciftci, N. S. Stability and Photodegradation Mechanisms of Conjugated Polymer/fullerene Plastic Solar Cells. *Sol. Energy Mater. Sol. Cells* **2000**, *61*, 35−42.
(29) Chambon, S.; Rivaton, A.; Gardette, J. L.; Firon, M. Photo- and Thermal Degradation of MDMO-PPV:PCBM Blends. *Sol. Energy Mater. Sol. Cells* **2007**, *91*, 394−398.
(30) Yamane, S.; Mizukado, J.; Suzuki, Y.; Sakurai, M.; Chen, L.; Suda, H. MALDI-TOF MS Study of the Photooxidation of PCBM and Its Suppression by P3HT. *Chem. Lett.* **2015**, *44*, 339−341.
(31) Eklund, P. C.; Rao, A. M.; Zhou, P.; Wang, Y.; Holden, J. M. Photochemical Transformation of $C_{60}$ and $C_{70}$ Films. *Thin Solid Films* **1995**, *257*, 185−203.
(32) Rao, A. M.; Wang, K.-A.; Holden, J. M.; Wang, Y.; Zhou, P.; Eklund, P. C.; Eloi, C. C.; Robertson, J. D. Photoassisted Oxygen Doping of C60 Films. *J. Mater. Res.* **1993**, *8*, 2277−2281.
(33) Matsuo, Y.; Ozu, A.; Obata, N.; Fukuda, N.; Tanaka, H.; Nakamura, E. Deterioration of Bulk Heterojunction Organic Photovoltaic Devices by a Minute Amount of Oxidized Fullerene. *Chem. Commun. (Cambridge, U. K.)* **2012**, *48*, 3878−3880.
(34) Wu, Y.; Zhang, G. Performance Enhancement of Hybrid Solar Cells Through Chemical Vapor Annealing. *Nano Lett.* **2010**, *10*, 1628−1631.
(35) Peet, J.; Kim, J. Y.; Coates, N. E.; Ma, W. L.; Moses, D.; Heeger, A. J.; Bazan, G. C. Efficiency Enhancement in Low-Bandgap Polymer Solar Cells by Processing with Alkane Dithiols. *Nat. Mater.* **2007**, *6*, 497−500.
(36) Ma, W.; Yang, C.; Gong, X.; Lee, K.; Heeger, A. J. Thermally Stable, Efficient Polymer Solar Cells with Nanoscale Control of the Interpenetrating Network Morphology. *Adv. Funct. Mater.* **2005**, *15*, 1617−1622.
(37) Yin, W.; Dadmun, M. A New Model for the Morphology of P3HT/PCBM Organic Photovoltaics from Small-Angle Neutron Scattering: Rivers and Streams. *ACS Nano* **2011**, *5*, 4756−4768.
(38) Jamieson, F. C.; Domingo, E. B.; McCarthy-Ward, T.; Heeney, M.; Stingelin, N.; Durrant, J. R. Fullerenecrystallisation as a Key Driver of Charge Separation in Polymer/fullerene Bulk Heterojunction Solar Cells. *Chem. Sci.* **2012**, *3*, 485−492.
(39) Wu, W.-R.; Jeng, U.-S.; Su, C.-J.; Wei, K.-H.; Su, M.-S.; Chiu, M.-Y.; Chen, C.-Y.; Su, W.-B.; Su, C.-H.; Su, A.-C. Competition between Fullerene Aggregation and Poly(3-Hexylthiophene) Crystallization upon Annealing of Bulk Heterojunction Solar Cells. *ACS Nano* **2011**, *5*, 6233−6243.
(40) Fernandes, L.; Gaspar, H.; Bernardo, G. Inhibition of Thermal Degradation of Polystyrene by C60 and PCBM: A Comparative Study. *Polym. Test.* **2014**, *40*, 63−69.
(41) Campbell, K.; Gurun, B.; Sumpter, B. G.; Thio, Y. S.; Bucknall, D. G. Role of Conformation in Π−π Interactions and Polymer/Fullerene Miscibility. *J. Phys. Chem. B* **2011**, *115*, 8989−8995.
(42) Bucknall, D. G.; Bernardo, G.; Shofner, M. L.; Nabankur, D.; Raghavan, D.; Sumpter, B. G.; Sides, S.; Huq, A.; Karim, A. Phase Morphology and Molecular Structure Correlations in Model Fullerene-Polymer Nanocomposites. *Mater. Sci. Forum* **2012**, *714*, 63−66.
(43) Huang, Y.; Wen, W.; Mukherjee, S.; Ade, H.; Kramer, E. J.; Bazan, G. C. High-Molecular-Weight Insulating Polymers Can Improve the Performance of Molecular Solar Cells. *Adv. Mater.* **2014**, *26*, 4168−4172.
(44) Zhu, Z.; Xue, Q.; He, H.; Jiang, K.; Hu, Z.; Bai, Y.; Zhang, T.; Xiao, S.; Gundogdu, K.; Gautam, B. R.; Ade, H.; Huang, F.; Wong, K. S.; Yip, H.-L.; Yang, S.; Yan, H. A PCBM Electron Transport Layer Containing Small Amounts of Dual Polymer Additives That Enables Enhanced Perovskite Solar Cell Performance. *Adv. Sci.* **2016**, *3*, 1500353.
(45) Richter, M. H.; Friedrich, D.; Schmeißer, D. Valence and Conduction Band States of PCBM as Probed by Photoelectron Spectroscopy at Resonant Excitation. *BioNanoSci.* **2012**, *2*, 59−65.
(46) Díaz, J.; Paolicelli, G.; Ferrer, S.; Comin, F. Separation of the Sp 3 and Sp 2 Components in the C1 *S* Photoemission Spectra of Amorphous Carbon Films. *Phys. Rev. B: Condens. Matter Mater. Phys.* **1996**, *54*, 8064−8069.
(47) Xin, H.; Subramaniyan, S.; Kwon, T.-W.; Shoaee, S.; Durrant, J. R.; Jenekhe, S. A. Enhanced Open Circuit Voltage and Efficiency of Donor−Acceptor Copolymer Solar Cells by Using Indene-C60 Bisadduct. *Chem. Mater.* **2012**, *24*, 1995−2001.
(48) Xiao, Z.; Yao, J.; Yang, D.; Wang, F.; Huang, S.; Gan, L.; Jia, Z.; Jiang, Z.; Yang, X.; Zheng, B.; Yuan, G.; Zhang, S.; Wang, Z. Synthesis of [59]Fullerenones through Peroxide-Mediated Stepwise Cleavage of Fullerene Skeleton Bonds and X-Ray Structures of Their Water-Encapsulated Open-Cage Complexes. *J. Am. Chem. Soc.* **2007**, *129*, 16149−16162.


DOI: 10.1021/acsami.7b03298
*ACS Appl. Mater. Interfaces* XXXX, XXX, XXX−XXX

(49) Cook, S.; Ohkita, H.; Kim, Y.; Benson-Smith, J. J.; Bradley, D. D. C.; Durrant, J. R. A Photophysical Study of PCBM Thin Films. *Chem. Phys. Lett.* **2007**, *445*, 276−280.
(50) Guilbert, A. A. Y.; Schmidt, M.; Bruno, A.; Yao, J.; King, S.; Tuladhar, S. M.; Kirchartz, T.; Alonso, M. I.; Goñi, A. R.; Stingelin, N.; Haque, S. A.; Campoy-Quiles, M.; Nelson, J. Spectroscopic Evaluation of Mixing and Crystallinity of Fullerenes in Bulk Heterojunctions. *Adv. Funct. Mater.* **2014**, *24*, 6972−6980.
(51) Neugebauer, H.; Brabec, C. J.; Hummelen, J. C.; Janssen, R. A. J.; Sariciftci, N. S. Stability Studies and Degradation Analysis of Plastic Solar Cell Materials by FTIR Spectroscopy. *Synth. Met.* **1999**, *102*, 1002−1003.
(52) Kettle, J.; Waters, H.; Ding, Z.; Horie, M.; Smith, G. C. Chemical Changes in PCPDTBT:PCBM Solar Cells Using XPS and TOF-SIMS and Use of Inverted Device Structure for Improving Lifetime Performance. *Sol. Energy Mater. Sol. Cells* **2015**, *141*, 139−147.
(53) National Institute of Standards and Technology. NIST X-ray Photoelectron Spectroscopy Database, Version 4.1 http://srdata.nist.gov/xps/ (accessed Oct 16, 2016).
(54) Benson-Smith, J. J.; Ohkita, H.; Cook, S.; Durrant, J. R.; Bradley, D. D. C.; Nelson, J. Charge Separation and Fullerene Triplet Formation in Blend Films of Polyfluorene Polymers with [6,6]-Phenyl C61 Butyric Acid Methyl Ester. *Dalt. Trans.* **2009**, *45*, 10000−10005.
(55) Chow, P. C. Y.; Albert-Seifried, S.; Gélinas, S.; Friend, R. H. Nanosecond Intersystem Crossing Times in Fullerene Acceptors: Implications for Organic Photovoltaic Diodes. *Adv. Mater.* **2014**, *26*, 4851−4854.
(56) Yasuda, T.; Tsutsui, T. Organic Field-Effect Transistors Based on High Electron and Ambipolar Carrier Transport Properties of Copper−phthalocyanine. *Chem. Phys. Lett.* **2005**, *402*, 395−398.
(57) Dattani, R.; Gibson, K. F.; Few, S.; Borg, A. J.; DiMaggio, P. A.; Nelson, J.; Kazarian, S. G.; Cabral, J. T. Fullerene Oxidation and Clustering in Solution Induced by Light. *J. Colloid Interface Sci.* **2015**, *446*, 24−30.
(58) Ohkita, H.; Cook, S.; Astuti, Y.; Duffy, W.; Heeney, M.; Tierney, S.; McCulloch, I.; Bradley, D. D. C.; Durrant, J. R. Radical Ion Pair Mediated Triplet Formation in Polymer−fullerene Blend Films. *Chem. Commun.* **2006**, *82*, 3939−3941.
(59) Faist, M. A.; Kirchartz, T.; Gong, W.; Ashraf, R. S.; McCulloch, I.; de Mello, J. C.; Ekins-Daukes, N. J.; Bradley, D. D. C.; Nelson, J. Competition between the Charge Transfer State and the Singlet States of Donor or Acceptor Limiting the Efficiency in Polymer:Fullerene Solar Cells. *J. Am. Chem. Soc.* **2012**, *134*, 685−692.
(60) Kraus, H.; Heiber, M. C.; Väth, S.; Kern, J.; Deibel, C.; Sperlich, A.; Dyakonov, V. Analysis of Triplet Exciton Loss Pathways in PTB7:PC71BM Bulk Heterojunction Solar Cells. *Sci. Rep.* **2016**, *6*, 29158.


DOI: 10.1021/acsami.7b03298
*ACS Appl. Mater. Interfaces* XXXX, XXX, XXX−XXX